Research Article Vol. 3, No. 6 / 15 Jun 2024 / Optics Continuum 1025
OPTICS CONTINUUM

Harmonic motion modes in parabolic GRIN fibers

A. Collado Hernández,[1] F. Marroquín Gutiérrrez,[2] and B. M. Rodríguez-Lara[2,3,4]

[1]*Facultad de Ciencias Físico Matemáticas, Universidad Autónoma de Nuevo León, San Nicolás de los Garza, 66455, Mexico*
[2]*Universidad Politécnica de Pachuca, Carr. Pachuca-Cd. Sahagún Km.20, Ex-Hda. Santa Bárbara, Zempoala, 43830, Hidalgo, Mexico*
[3]*bmlara@upp.edu.mx*
[4]*blas.rodriguez@gmail.com*

Abstract: We report electromagnetic field modes solving the inhomogeneous Maxwell equations for parabolic gradient index fibers in the low refractive index contrast approximation. The first family comprises accelerating fields characterized by an intensity distribution center tracing a circular trajectory transverse to the fiber optical axis. These fields maintain an invariant shape for both their intensity and phase distributions while rotating around their center. The second family comprises breathing fields characterized by an intensity distribution center aligned with the fiber optical axis. These fields exhibit intensity distribution scaling along propagation, while their phase swirls and rotates around the optical axis without changing their intensity distribution shape and topological charge.

1. Introduction

Parabolic graded refractive index (GRIN) fibers [1,2] have a smoothly varying refractive index profile that decreases radially from the fiber axis, providing reduced modal dispersion compared to step-index fibers [3,4]. Their normal modes are well-understood with the analytic description of their spatial shape, propagation constants, and cladding-mode cutoffs in the so-called weak guidance approximation [5,6] as well as in full vector analysis [7,8]. Beyond telecommunications, they find utility in strain and temperature sensing [9,10], as well as medical imaging [11,12] to mention a few examples.

In the ideal scenario of infinite parabolic GRIN media, the propagation of Hermite- and Laguerre- [13–15], as well as Ince-Gauss [16] modes have been studied, using tools from classical and quantum physics [17,18], leading to the discovery of breathing helical phase vortex for Laguerre- [19], Bessel- [20], and Hermite-Gauss [21] modes, hypergeometric breathing modes [22], optical analogies of coherent states [23] and chirp induced breathing for Airy- [24] and Hermite-Gauss [25] modes, self-imaging for Airy-Gauss beams [26], so-called pendulum-type modes [27], and self-healing of Hermite-Gauss modes [28].

Harmonic motion, a fundamental concept in both classical and quantum physics, describes the oscillatory movement of systems where the restoring force is proportional to the displacement from equilibrium, characteristic of harmonic oscillators with their periodic oscillations. We extend this idea to optical physics by focusing on realistic low-contrast parabolic GRIN fibers to propose electromagnetic field modes that solve Maxwell equations for inhomogeneous media in the weak guidance approximation, exhibiting periodic oscillations. In Section 2, we show that the Sturm-Liouville eigenvalue problem in the fiber core is a finite analogue to an ideal two-dimensional quantum harmonic oscillator. We construct analytic propagation invariant modes with constant radial and azimuthal numbers, find their propagation constants and cut-off relations that are in good agreement with numerical results from finite element method (FEM).

#525575 https://doi.org/10.1364/OPTCON.525575
Journal © 2024 Received 9 Apr 2024; revised 13 May 2024; accepted 15 May 2024; published 14 Jun 2024

OPTICS CONTINUUM

In Section 3, we identify symmetries related to the conservation of circular and azimuthal numbers to introduce two families of harmonic motions modes. We built these as the coherent superposition of propagation invariant modes, drawing an analogy to coherent states in quantum optics. One family comprises accelerating light fields, whose intensity distribution center follows a circular trajectory in the plane transverse to propagation, Sec. 4. The other family consists of breathing light fields, whose intensity distribution center follows the propagation axis and their width varies with propagation, Sec. 5. We conclude our findings in Sec. 6.

2. Propagation invariant modes

Consider a parabolic GRIN fiber characterized by a refractive index [2],

$$n(\rho) = n_{\text{cl}} + \Delta n f(\rho), \qquad f(\rho) = \begin{cases} 1 - \frac{\rho^2}{a^2}, & 0 \le \rho \le a, \\ 0, & \rho > a, \end{cases} \tag{1}$$

where the core of radius a has maximum refractive index $n_{\text{max}} = n(0) = n_{\text{cl}} + \Delta n$ at its optical axis. The cladding has constant refractive index n_{cl}, resulting in a refractive index contrast $\Delta n = n_{\text{max}} - n_{\text{cl}}$. For low refractive index contrast, $\Delta n / n_{\text{cl}} \ll 1$, we use the weak guidance approximation [29] to propose propagation invariant transverse electromagnetic fields,

$$\begin{aligned} \mathbf{E} &\approx \hat{\mathbf{e}} |E| e^{i\theta} \Psi(\rho, \varphi) e^{i(\beta z - \omega t)}, \\ \mathbf{B} &\approx (\hat{\mathbf{z}} \times \hat{\mathbf{e}}) \frac{n(\rho)}{c} |E| e^{i\theta} \Psi(\rho, \varphi) e^{i(\beta z - \omega t)}, \end{aligned} \tag{2}$$

that solve Maxwell equations for an inhomogeneous medium [30]. The fields are given in terms of the unit polarization vector $\hat{\mathbf{e}}$, real field amplitude $|E|$ with phase θ, speed of light in vacuum c with field frequency ω, propagation constant β, low contrast approximated refractive index,

$$n^2(\rho) \approx n_{\text{cl}}^2 + 2\Delta n f(\rho), \tag{3}$$

and scalar wave function,

$$\Psi_{p,\ell}(\rho, \varphi) = A \begin{cases} \psi_{p,\ell}(\rho, \varphi) & 0 \le \rho \le a, \\ \frac{\psi_{a,\ell}(a,\varphi)}{K_{|\ell|}(\alpha a)} K_{|\ell|}(\alpha \rho) e^{i\ell\varphi} & \rho > a, \end{cases} \tag{4}$$

solving the Sturm-Liouville eigenvalue problem,

$$\left[\nabla_t^2 + 2k_0^2 n_{\text{cl}} \Delta n f(x_1, x_2) - \beta^2 + k_0^2 n_{\text{cl}}^2\right] \Psi(x_1, x_2) = 0, \tag{5}$$

a finite-dimensional analogy of the two-dimensional quantum harmonic oscillator, in terms of Laguerre-Gauss modes,

$$\psi_{p,\ell}(\rho, \varphi) = (-1)^p \sqrt{\frac{p!}{\pi(p + |\ell|)!}} \left(\frac{\rho}{\sigma}\right)^{|\ell|} e^{-\frac{\rho^2}{2\sigma^2}} \mathrm{L}_p^{|\ell|}\left(\frac{\rho^2}{\sigma^2}\right) e^{i\ell\varphi}, \tag{6}$$

with generalized Laguerre polynomials $\mathrm{L}_n^{(\gamma)}(x)$, constant Gaussian waist,

$$\sigma^2 = \frac{a}{k_0} \sqrt{\frac{1}{2 n_{\text{cl}} \Delta n}}, \tag{7}$$

and propagation constant,

$$\beta^2(p, \ell) = k_0^2 n_{\text{cl}} (n_{\text{cl}} + 2\Delta n) - \frac{2}{\sigma^2} (2p + |\ell| + 1), \tag{8}$$

with radial and azimuthal number values $p = 0, 1, 2, \ldots$ and $\ell = 0, \pm 1, \pm 2, \ldots$, in that order. The solution in the cladding is given in terms of modified Bessel functions of the second kind $K_\gamma(x)$

OPTICS CONTINUUM

with auxiliary propagation constant,

$$\alpha^2 = 2k_0^2 n_{\rm cl}\Delta n - \frac{2}{\sigma^2}(2p + |\ell| + 1), \tag{9}$$

vacuum wave number $k_0 = 2\pi/\lambda_0$, and vacuum wavelength λ_0. These propagation constants provide the cut-off relation,

$$k_0 a \geq \sqrt{\frac{2}{n_{\rm cl}\Delta n}}\,(2p + |\ell| + 1)\,, \tag{10}$$

for the number of modes supported by a particular fiber. We choose the normalization parameter A to provide,

$$\int d^2 r\, \Psi^*_{p',\ell'}(\rho,\varphi)\Psi_{p,\ell}(\rho,\varphi) = \delta_{p,p'}\delta_{\ell,\ell'}, \tag{11}$$

orthonormal modes. Figure 1 shows the three modes supported by a parabolic GRIN fiber with cladding refractive index $n_{\rm cl} = 1.444$, refractive index contrast $\Delta n = 0.05$, and core radius $a = 1.058\,\mu$m for free space wavelength $\lambda_0 = 632\,$nm calculated using FEM simulation that are in good agreement with our exact analytic result in Eq. (8), $\beta(0,0) = 1.460 \times 10^7\,\text{rad}\cdot\text{m}^{-1}$ [$\beta_{FEM}(0,0) = 1.461 \times 10^7\,\text{rad}\cdot\text{m}^{-1}$] and $\beta(0,\pm1) = 1.436 \times 10^7\,\text{rad}\cdot\text{m}^{-1}$ [$\beta_{FEM}(0,\pm1) = 1.439 \times 10^7\,\text{rad}\cdot\text{m}^{-1}$], up to a rotation of the reference frame.

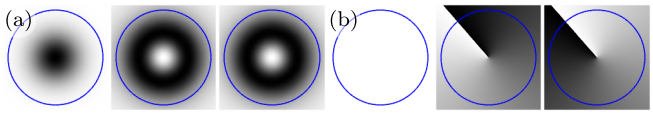

Fig. 1. (a) Intensity $|\Psi_{p,\ell}(\rho,\varphi)|^2$, and (b) phase $\arg\left[\Psi_{p,\ell}(\rho,\varphi)\right]$ distributions for the three modes, $p = 0, \ell = 0, \pm1$, supported by a parabolic GRIN fiber with cladding refractive index $n_{\rm cl} = 1.444$, refractive index contrast $\Delta n = 0.05$, and core radius $a = 1.058\,\mu$m shown in blue, for free space wavelength $\lambda_0 = 632\,$nm provided by FEM.

3. Harmonic motion modes

The normal modes in the core are the optical equivalent of the homogeneous, two-dimensional harmonic oscillator Laguerre-Gauss modes. Thus, we build electromagnetic field modes,

$$\begin{aligned} \mathbf{E} &\approx\ \hat{\mathbf{e}}|E|e^{i\theta}\Phi_{\pm}(k,\delta;\rho,\varphi,z)e^{-i\omega t}, \\ \mathbf{B} &\approx\ (\hat{\mathbf{z}}\times\hat{\mathbf{e}})\,\frac{n(\rho)}{c}|E|e^{i\theta}\Phi_{\pm}(k,\delta;\rho,\varphi,z)e^{-i\omega t}, \end{aligned} \tag{12}$$

with polarization that remains invariant to propagation and in terms of scalar wave functions,

$$\Phi_{\pm}(k,\delta;\rho,\varphi,z) = A\sum_{m=0}^{\infty}\sqrt{P(k,m,\delta)}\,\Psi_{p,\pm\ell}(\rho,\varphi)e^{i\beta(p,\pm\ell)z}, \tag{13}$$

that are the superposition of propagation invariant modes weighted by a probability distribution where radial and azimuthal numbers may depend on the summation index m; that is, $p \equiv p(k,m)$ and $\ell \equiv \ell(k,m)$. The probability distribution dictates the number of involved modes, while our cut-off relation provides us with the fiber radius size needed to support them. In addition, we

OPTICS CONTINUUM

approximate our analytic propagation constant in Eq. (8),

$$\begin{aligned}\beta(p,\ell) &\approx \beta_0 - \beta_1(p,\ell),\\ \beta_0 &= k_0\sqrt{n_{\rm cl}\,(n_{\rm cl}+2\Delta n)},\\ \beta_1(p,\ell) &= \frac{1}{a}\sqrt{\frac{2\Delta n}{n_{cl}+2\Delta n}}\;(2p+|\ell|+1)\,,\end{aligned} \tag{14}$$

in order to simplify our analysis. Our approximation holds for parameter values satisfying,

$$\frac{4\Delta n\,(2p+|\ell|+1)}{a^2\,(n_{\rm cl}+2\Delta n)} \ll 1, \tag{15}$$

where the core radius is key in ensuring its validity by balancing the contribution of higher-order field modes.

4. Accelerating modes

In the two-dimensional quantum harmonic oscillator, circular numbers, n_+ and n_-, define the radial and azimuthal numbers, $p = \min(n_+, n_-)$ and $\ell = n_+ - n_-$. Subspaces with constant circular numbers $n_\pm$ exhibit an underlying Heisenberg-Weyl symmetry [31]. Following the Glauber-Suddarshan coherent states [32,33] recipe yields a Poisson probability distribution, radial, and azimuthal numbers,

$$\begin{aligned}P(m,\delta) &= e^{-|\delta|^2}\frac{|\delta|^{2m}}{m!},\\ p(k,m) &= \min(k,m),\\ \ell(k,m) &= \pm(k-m),\end{aligned} \tag{16}$$

where the complex parameter δ amplitude and phase provide the intensity distribution center radial and angular displacement, respectively, in the plane transverse to propagation. These states have topological charge equal to $\ell = \pm k$.

It is simpler to generate insight using the mode with $k = 0$,

$$\Phi_\pm(0,\delta;\rho,\varphi,z) = \frac{A}{\sqrt{\pi}}e^{-\frac{|\delta(z)|^2}{2}}e^{-\frac{\rho}{\sigma}\tilde{\delta}(z)}e^{-\frac{\rho^2}{2\sigma^2}}, \quad \rho \le a, \tag{17}$$

with modified complex parameter,

$$\tilde{\delta}(z) = \delta e^{i\beta_1(0,0)z}, \tag{18}$$

that takes the form of a displaced Gaussian scalar wave within the core. The intensity distribution center locates at the radial distance,

$$\rho_0 = \int_0^\infty \rho d\rho \int_0^{2\pi} d\varphi\;\rho|\Phi_\pm(k,\delta;\rho,\varphi,z)|^2, \tag{19}$$

in terms of the modified Bessel function of the first kind $I_\gamma(x)$. It is straightforward to see that the intensity distribution center follows an helical trajectory with constant radius $\rho_0(z) = \rho_0$, and angular position $\varphi_0(z) = \arg(\delta) - \beta(0,0)z$ proportional to the propagation distance. Its intensity and phase distributions in the plane transverse to propagation rotate around the point defined by these functions. Figure 2(a) shows Poisson probability distribution for a parameter $\delta = 4$. It is enough to consider the first fifty modes $m \in [0, 50]$ to construct our states. Considering a parabolic GRIN fiber with cladding refractive index $n_{\rm cl} = 1.444$ and refractive

OPTICS CONTINUUM

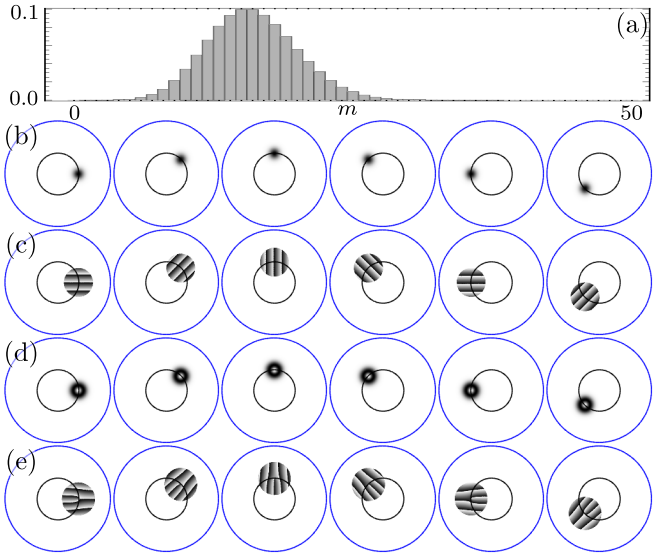

Fig. 2. (a) Poisson probability distribution $P(m, \delta)$ for a parameter $\delta = 4$. (b) [(c)] Intensity and (d) [(e)] phase distribution for our harmonic motion mode with topological charge $k = 0$ [$k = 1$] at propagation distances $\beta_1(0, 0)z = 0, \pi/4, \pi/2, 3\pi/4, \pi, 5\pi/4$ from left to right. Core radius $a = 28.058\,\mu$m shown in blue and radial displacement $\rho_0(z) = 11.072\,\mu$m [$\rho_0(z) = 11.246\,\mu$m] in black.

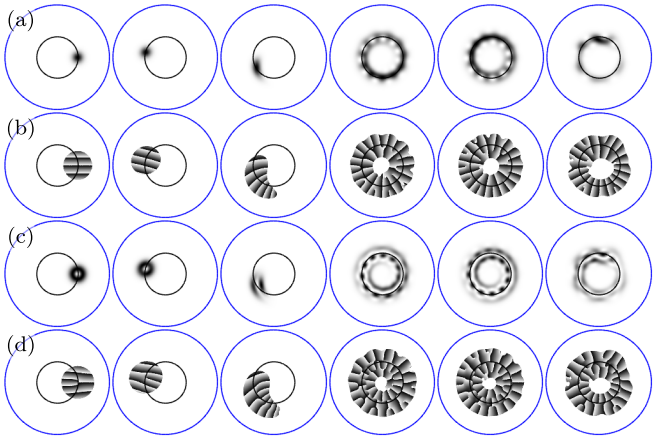

Fig. 3. (a) [(c)] Intensity and (b) [(d)] phase distribution for our harmonic motion mode in Fig. 2 at propagation distances $z = 0, 0.001, 0.01, 0.1, 1, 10$ m from left to right.

OPTICS CONTINUUM

index contrast $\Delta n = 0.05$ for free space wavelength $\lambda_0 = 632$ nm, yields a minimum core radius $a = 28.058\mu$m for a fiber supporting topological charges $k = 0, 1$. The maximum absolute error between the analytic and approximated propagation constant for these parameters and modes $\beta = |\beta(k, 50) - \beta_0 + \beta_1(k, 50)|/\beta(k, 50) \approx 5 \times 10^{-4}$ is negligible. Figure 2(b) [Fig. 2(d)] shows the intensity and Fig. 2(c) [Fig. 2(e)] the phase distributions for our harmonic motion mode with topological charge $\ell = k = 0$ [$\ell = k = 1$] at small propagation distances $\beta_1(0, 0)z = 0, \pi/4, \pi/2, 3\pi/4, \pi, 5\pi/4$. For short propagation distances, Figs. 2, our accelerating modes maintain their intensity distribution shape, with their centroid tracing a helical path; a characterstic behaviour of so-called accelerating light beams [34]. Our results suggests that, with increased propagation distances, Fig. 3, our accelerating modes undergo deformation. Using fiber cores with a larger radius help mitigating this issue.

5. Breathing modes

Subspaces with constant azimuthal number ℓ exhibit an underlying symmetry provided by the $su(1, 1)$ algebra [31]. Following the Gilmore-Perelomov coherent states [35,36] recipe yields a probability distribution, radial and azimuthal numbers,

$$\begin{aligned} P([m, \delta) &= \frac{(2k + m - 1)!}{m!(2k - 1)!} \operatorname{sech}^{4k}\frac{|\delta|}{2} \left| -\frac{\delta}{|\delta|} \tanh\frac{|\delta|}{2} \right|^{2m}, \\ p(k, m) &= m, \\ \ell(k, m) &= \pm(2k - 1), \end{aligned} \tag{20}$$

with Bargmann parameter $k = 1/2, 1, 3/2, \ldots$ These states take the form of a Gaussian envelope times the radial coordinate raised to the power of the azimuthal number,

$$\begin{aligned} \Phi_\pm(k, \delta; \rho, \varphi, z) = \frac{A e^{i[\beta_0 z - i2k\beta_1(0,0)z]}}{\sqrt{\pi(2k - 1)!}\, w(\delta, z)^{2k}} \left(\frac{\rho}{\sigma}\right)^{2k-1} \times \\ \times e^{-\frac{\rho^2}{2\sigma^2 w^2}} e^{i\phi_\pm(\delta,z)}, \quad \rho \le a, \end{aligned} \tag{21}$$

within the core. The Gaussian envelope waist and overall phase,

$$\begin{aligned} w^2(\delta, z) &= \cosh|\delta| - \cos\{\arg[\tilde{\delta}(z)]\} \sinh|\delta|, \\ \phi_\pm(\delta, z) &= \pm(2k - 1)\varphi - \sin\{\arg[\tilde{\delta}(z)]\} \sinh|\delta| \frac{\rho^2}{w^2\sigma^2}, \end{aligned} \tag{22}$$

in that order, in terms of the modified parameter, and modified parameter,

$$\tilde{\delta}(z) = \delta e^{-i2\beta_1(0,0)z} \tag{23}$$

show that the intensity distribution width varies with propagation, expanding and contracting, while the pase exhibits a topological charge $\ell = \pm(2k - 1)$. The phase distribution is a function of the radial coordinate and propagation distance, transitioning from a standard to a swirl vortex with propagation, all while rotating around the fiber optical axis. Figure 4(a) [Fig. 4(d)] shows the intensity distribution for a parameter $\delta = 2$. It is enough to consider the first twenty modes $m \in [0, 20]$ to construct our states. Using the same fiber yields a minimum core radius $a = 22.235\mu$m for a fiber supporting topological charges $k = 0, 1$. The maximum absolute error between the analytic and approximated propagation constant for these parameters and modes $\beta = |\beta(k, 50) - \beta_0 + \beta_1(k, 50)|/\beta(k, 50) \approx 4 \times 10^{-3}$ is negligible. Figure 3(b) [Fig. 3(e)] shows the intensity and Fig. 3(c) [Fig. 3(f)] the phase distributions for our harmonic motion mode with topological charge $\ell = 2k - 1 = 0$ [$\ell = 2k - 1 = 1$] at small propagation distances

OPTICS CONTINUUM

$\beta_1(0,0)z = 0, \pi/4, \pi/2, 3\pi/4, \pi, 5\pi/4$. The intensity distribution centroid of our breathing modes stays on the propagation axis with their shape scaling up and down. Our results suggest that these modes undergo deformation with larger propagation distances, Fig. 5. However, it is not easy to spot visually the deformation. The fact that they are the superposition of modes with identical topological charge may help mitigating this issue.

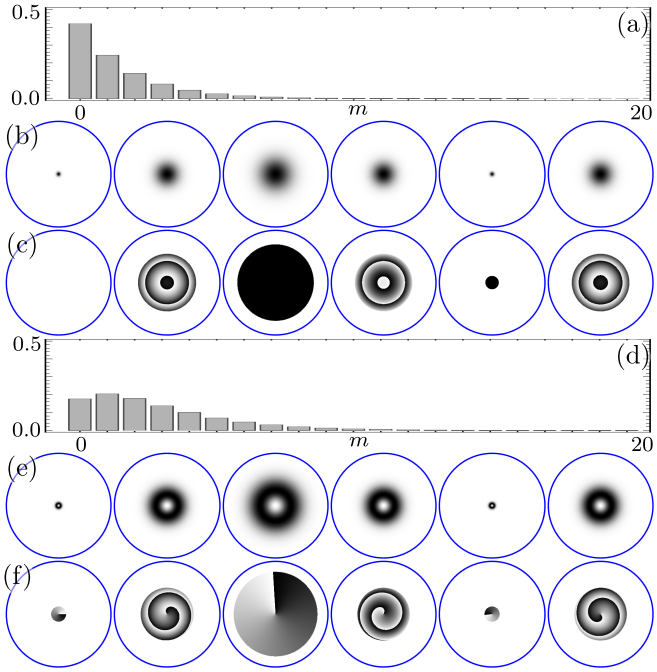

Fig. 4. (a)[(d)] Probability distribution $P(m, \delta)$ for a parameter $\delta = 2$. (b) [(e)] Intensity and (d) [(f)] phase distribution for our harmonic motion mode with topological charge $k = 1/2$ [$k = 1$] at propagation distances $\beta_1(0,0)z = 0, \pi/4, \pi/2, 3\pi/4, \pi, 5\pi/4$ from left to right. Core radius $a = 22.235\ \mu$m shown in blue.

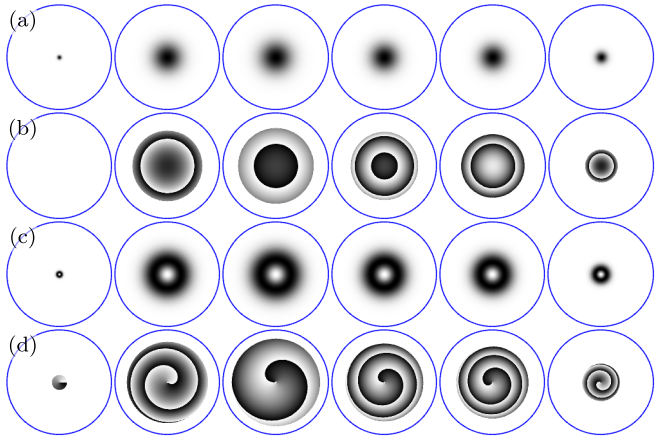

Fig. 5. (a) [(c)] Intensity and (b) [(d)] phase distribution for our harmonic motion mode in Fig. 4 at propagation distances $z = 0, 0.001, 0.01, 0.1, 1, 10$ m from left to right.

OPTICS CONTINUUM

In the same subspaces, following the Barut-Girardello coherent state [37] recipe yields a probability distribution, radial and azimuthal numbers,

$$\begin{aligned} P(k,m,\delta) &= \frac{|\delta|^{(2k+2m-1)}}{(2k-1)!\,m!\,\mathrm{I}_{2k-1}(2|\delta|)}, \\ p(k,m) &= m, \\ \ell(k,m) &= \pm(2k-1), \end{aligned} \tag{24}$$

with Bargmann parameter $k = 1/2, 1, 3/2, \ldots$ These states take the form of a Bessel-Gauss scalar wave function,

$$\begin{aligned} \Phi_{\pm}(k,\delta;\rho,\varphi,z) = {} & \frac{A(-1)^{-k+\frac{1}{2}}e^{-\tilde{\delta}(z)}}{\sqrt{\pi\,\mathrm{I}_{2k-1}(2|\delta|)}} e^{i[\beta_0 - i2k\beta_1(0,0)]z} e^{-\frac{\rho^2}{2\sigma^2}} \times \\ & \times \mathrm{J}_{2k-1}\left[\frac{2\sqrt{-\tilde{\delta}(z)}}{\sigma}\rho\right] e^{\pm i(2k-1)\varphi},\ \rho \le a, \end{aligned} \tag{25}$$

within the core in terms of the Bessel function of the first kind $\mathrm{J}_\gamma(x)$ with complex argument,

$$\tilde{\delta}(z) = \delta e^{-i2\beta_1(0,0)z}. \tag{26}$$

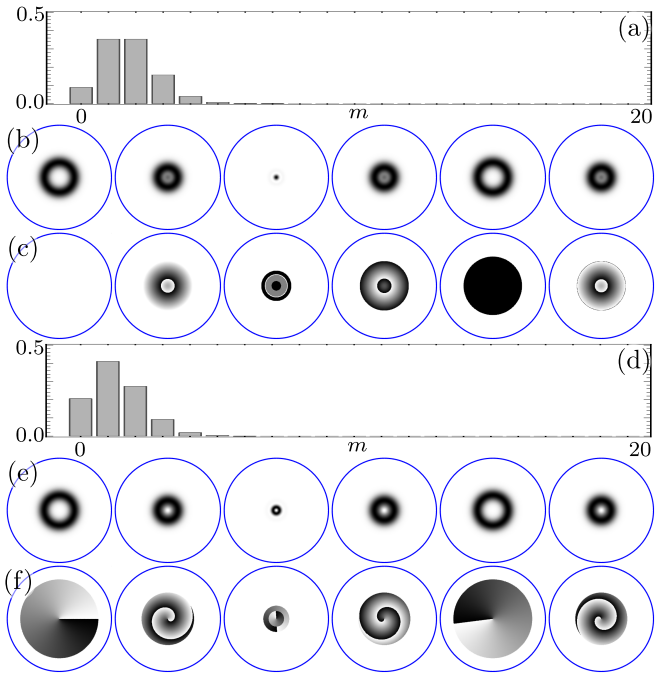

Fig. 6. Same as Fig. 4 for Bessel-Gauss mode.

It is not straightforward to see, but the intensity distribution width varies with propagation, expanding and contracting, while the phase shows a topological charge $\ell = \pm(2k-1)$. The phase distribution of the Bessel function with complex argument depends on the radial coordinate and propagation distance, transitioning from a standard to a swirl vortex with propagation, all while rotating around the fiber optical axis. Figure 6(a) [Fig. 6(d)] shows the probability distribution

OPTICS CONTINUUM

using the same fiber as before. Figure 6(b) [Fig. 6(e)] shows the intensity and Fig. 6(c) [Fig. 6(f)] the phase distributions for our harmonic motion mode with topological charge $\ell = 2k - 1 = 0$ [$\ell = 2k - 1 = 1$] at small propagation distances $\beta_1(0,0)z = 0, \pi/4, \pi/2, 3\pi/4, \pi, 5\pi/4$. Larger propagation distances follow the results presented in Fig. 5.

6. Conclusion

In summary, we reviewed the propagation invariant transverse electromagnetic field modes in parabolic GRIN fiber with finite radius within the weak guidance approximation, providing their propagation constant and cut-off relation. We showed that low-contrast parabolic GRIN fibers support field modes akin to coherent and squeezed states for two intrinsic symmetries involving circular and radial number conservation.

We introduced two families of harmonic motion field modes. The first family exhibits an intensity and phase distribution center that follows helical trajectories with constant radius during propagation while remaining shape invariant. The second family shows a varying intensity distribution width through propagation, maintaining its shape and topological charge while its phase distribution transitions from standard to swirl vortex. Our analysis indicates that larger core radii yield a closer match between numerical FEM and approximated analytic propagation constants, enabling our harmonic motion fields to propagate over longer distances without distortion. For instance, a fiber core radius of $a = 1$ mm allows for propagation distances of a few meters, obviating the crosstalk induced by fiber deformations.

Our theoretical proposal may be experimentally validated using digital holographic techniques. A low-power laser beam, expanded and collimated, illuminates a Spatial Light Modulator where a digital hologram of our harmonic motion modes reconstructs the optical field in the first diffraction order of a 4F optical system [31]. These light fields may then be coupled into a commercial parabolic GRIN fiber, following methodologies similar to those in recent structured light propagation experiments [27,28].

Furthermore, our harmonic motion modes serve as an optical analogy to quantum coherent states, linked to the Heisenberg-Weyl and the special unitary $su(1,1)$ Lie algebras of the two-dimensional quantum harmonic oscillator. These modes retain the statistical properties of their quantum counterparts, offering potential applications in areas like sensing and measurement [38,39]. Additionally, they present an opportunity for exploration in other physical systems that exhibit propagation-invariant or accelerating waves, such as surface plasmon polaritons and hydrodynamic waves.

Appendix: Coherent states for the isotropic two-dimensional quantum harmonic oscillator

The ideal isotropic two-dimensional quantum harmonic oscillator [40],

$$\hat{H} = \hbar\omega \frac{1}{2} \sum_{j=x,y} \left(\hat{p}_j^2 + \hat{q}_j^2 \right), \tag{27}$$

with dimensionless canonical variables $\hat{q}_j = \sqrt{m\omega/\hbar}\,\hat{x}_j$ and $\hat{p}_j = \sqrt{1/(\hbar m\omega)}\,\hat{p}_{x_j} = -i\partial_{q_j}$ with $\hat{x}_j = \hat{x}, \hat{y}$ [41], admits Laguerre-Gauss modes,

$$\hat{H}\psi_{p,\ell}(\rho,\varphi) = \hbar\omega\,(2p + |\ell| + 1)\,\psi_{p,\ell}(\rho,\varphi), \tag{28}$$

as eigenmodes in polar configuration space [42].

OPTICS CONTINUUM

Introducing left- and right-circular modes [40],

$$\hat{a}_{\pm}^{\dagger} = \frac{1}{\sqrt{2}}\left(\hat{a}_x^{\dagger} \pm i\hat{a}_y^{\dagger}\right), \tag{29}$$

proportional to the standard creation (annihilation) operator, $\hat{a}_j^{\dagger} = \left(\hat{q}_j - i\hat{p}_j\right)/\sqrt{2}$ ($\hat{a}_j = \left(\hat{q}_j + i\hat{p}_j\right)/\sqrt{2}$) with $j = x, y$, provides a Heisenberg–Weyl algebra,

$$\left[\hat{a}_j, \hat{a}_k^{\dagger}\right] = \delta_{j,k}, \tag{30}$$

with $j, k = \pm$, that allows the construction of Glauber–Sudarshan coherent states [32,33],

$$\begin{aligned} |\alpha_+, \alpha_-\rangle &= \prod_{j=\pm} e^{-\left(\alpha_j \hat{a}_j^{\dagger} - \alpha_j^* \hat{a}_j\right)}|0\rangle, \\ &= e^{-\frac{1}{2}\left(|\alpha_+|^2 + |\alpha_-|^2\right)} \sum_{k,l=0}^{\infty} \frac{\alpha_+^k \alpha_-^l}{\sqrt{k!l!}}|k, l\rangle, \end{aligned} \tag{31}$$

for each circular mode, where we use the vector notation,

$$\langle \rho, \varphi | n_+, n_-\rangle = \psi_{p(n_+,n_-),\ell(n_+,n_-)}(r, \phi), \tag{32}$$

with

$$\begin{aligned} p(n_+, n_-) &= \min(n_+, n_-), \\ \ell(n_+, n_-) &= n_+ - n_-, \end{aligned} \tag{33}$$

These coherent states relate to the multiplication of two Poisson probability distributions,

$$P\left(\{j, k\}, \{\alpha_+, \alpha_-\}\right) = e^{-\left(|\alpha_+|^2 + |\alpha_-|^2\right)} \frac{|\alpha_+|^{2k}|\alpha_-|^{2l}}{k!l!}, \tag{34}$$

and minimize uncertainty relations for each dimensionless canonical pair,

$$\Delta\hat{q}_j \Delta\hat{p}_j = \frac{1}{2}, \tag{35}$$

with $j = x, y, \pm$, making them good candidates for measurement and sensing applications [38].

Additionally, the oscillator possess an underlying two-mode representation of the Lie algebra $su(1,1)$ [43–45],

$$\begin{aligned} \hat{K}_+ &= \hat{a}_+^{\dagger}\hat{a}_-^{\dagger}, \\ \hat{K}_- &= \hat{a}_+\hat{a}_-, \\ \hat{K}_0 &= \frac{1}{2}\left(\hat{a}_+^{\dagger}\hat{a}_+ + \hat{a}_-^{\dagger}\hat{a}_- + 1\right), \\ \hat{K}^2 &= \frac{1}{4}\left[\left(\hat{a}_+^{\dagger}\hat{a}_+ - \hat{a}_-^{\dagger}\hat{a}_-\right)^2 - 1\right], \end{aligned} \tag{36}$$

given in terms of the circular creation and annihilation operators such that,

$$\begin{aligned} \left[\hat{K}_+, \hat{K}_-\right] &= -2\hat{K}_0, \\ \left[\hat{K}_0, \hat{K}_\pm\right] &= \pm\hat{K}_\pm, \\ \left[\hat{K}^2, \hat{K}_j\right] &= 0, \end{aligned} \tag{37}$$

with $j = 0, \pm$. This symmetry allows the partition of the Hilbert space defined by Laguerre-Gauss modes into infinite dimensional subspaces comprising states that are eigenstates of the Casimir

OPTICS CONTINUUM

operator $\hat{K}^2$ with eigenvalues $k(k-1)$; that is, their Bargmann parameter takes half-integer values $k = (|\ell|+1)/2 = 1/2, 1, 3/2, \ldots$ and is double degenerate to account for the sign of the azimuthal number, except for $\langle\hat{\ell}\rangle = 0$.

The Gilmore–Perelomov coherent states [35,36] for each one of this subspaces,

$$\begin{aligned} |k;\zeta,\theta\rangle_{\pm} &= e^{-\frac{zeta}{2}\left(e^{-i\theta}\hat{K}_{+}-e^{i\theta}\hat{K}_{-}\right)}|k;0\rangle, \\ &= \left(1-\left|\tanh\frac{\zeta}{2}\right|^2\right)^{k}\sum_{m=0}^{\infty}\sqrt{\frac{\Gamma(2k+m)}{m!\Gamma(2k)}}\times \\ &\times\left(-e^{-i\theta}\tanh\frac{\zeta}{2}\right)^{m}|k;m\rangle\,, \end{aligned} \tag{38}$$

where we use the vector notation,

$$\langle\rho,\varphi|k;m\rangle = \psi_{m,\pm(2k-1)}(\rho,\varphi), \tag{39}$$

are a coherent superposition of Laguerre-Gauss modes with identical topological phase. These coherent states, known in quantum optics as two-mode squeezed states [46], relate to the probability distribution,

$$P\left(k,m,\zeta e^{i\theta}\right) = \left(1-\left|\tanh\frac{\zeta}{2}\right|^2\right)^{2k}\frac{\Gamma(2k+m)}{m!\Gamma(2k)}\tanh^{2m}\frac{\zeta}{2}. \tag{40}$$

In these squeezed states, the uncertainty of certain linear combinations of canonical pair elements at the expense of their commutative pair, making them good candidates for measurement and sensing applications [39]. The same happens with the Barut–Girardello coherent states,

$$\hat{K}_{-}|k;\xi\rangle = \xi|k;\xi\rangle, \tag{41}$$

for each one of this subspaces [37,44],

$$|k;\xi\rangle = \frac{\xi^{k-\frac{1}{2}}}{\sqrt{\mathrm{I}_{2k-1}(2|\xi|)}}\sum_{m=0}^{\infty}\frac{\xi^{m}}{\sqrt{m!\Gamma(2k+m)}}\,|k;m\rangle\,, \tag{42}$$

related to the probability distribution,

$$P\left(k,m,\zeta e^{i\theta}\right) = \frac{|\xi|^{2(k+m)-1}}{m!\Gamma(2k+m)\mathrm{I}_{2k-1}(2|\xi|)}. \tag{43}$$

Further information on the optical analogy of quantum coherent states for the diverse underlying symmetries of the isotropic two-dimensional quantum harmonic oscillator may be found in Ref. [31] and references therein.

Funding. Consejo Nacional de Humanidades, Ciencias y Tecnologías (841625).

Acknowledgments. B. M. R.-L. thanks Dilia Aguirre Olivas, Gabriel Mellado-Villaseñor, Benjamin Raziel Jaramillo Avila, Zulema Gress Mendoza, and Benjamin Perez-Garcia for fruitful discussions.

Disclosures. The authors declare no conflicts of interest.

Data availability. Data underlying the results presented in this paper may be obtained from the authors upon reasonable request.

OPTICS CONTINUUM

References

1. W. Streifer and C. N. Kurtz, "Scalar analysis of radially inhomogeneous guiding media," J. Opt. Soc. Am. **57**(6), 779–786 (1967).
2. D. Marcuse, "The impulse response of an optical fiber with parabolic index profile," Bell Syst. Tech. J. **52**(7), 1169–1174 (1973).
3. F. W. Ostermayer Jr. and D. A. Pinnow, "Optimum refractive-index difference for graded-index fibers resulting from concentration-fluctuation scattering," Bell Syst. Tech. J. **53**(7), 1395–1402 (1974).
4. L. G. Cohen, P. Kaiser, and J. B. M. Chesney, "Transmission properties of a low–loss near–parabolic–index fiber," Appl. Phys. Lett. **26**(8), 472–474 (1975).
5. R. Yamada, T. Meiri, and N. Okamoto, "Guided waves along an optical fiber with parabolic index profile," J. Opt. Soc. Am. **67**(1), 96–103 (1977).
6. B. K. Garside, T. K. Lim, and J. P. Marton, "Propagation characteristics of parabolic-index fiber modes: linearly polarized approximation," J. Opt. Soc. Am. **70**(4), 395–400 (1980).
7. M. Hashimoto, S. Nemoto, and T. Makimoto, "Analysis of guided waves along the cladded optical fiber: Parabolic-index core and homogeneous cladding," IEEE Trans. Microwave Theory Tech. **25**(1), 11–17 (1977).
8. T. K. Lim, B. K. Garside, and J. P. Marton, "Guided modes in fibres with parabolic-index core and homogeneous cladding," Opt. Quantum Electron. **11**(4), 329–344 (1979).
9. S. M. Tripathi, A. Kumar, and R. K. Varshney, "Strain and temperature sensing characteristics of single–mode–multimode–single–mode structures," J. Lightwave Technol. **27**(13), 2348–2356 (2009).
10. F. Beltrán-Mejía, C. R. Biazoli, and C. M. B. Cordeiro, "Tapered GRIN fiber microsensor," Opt. Express **22**(25), 30432–30441 (2014).
11. M. A. Bolshtyansky and B. Y. Zel'dovich, "Stabilization of transmission function: theory for an ultrathin endoscope of one multimode fiber," Appl. Opt. **36**(16), 3673–3681 (1997).
12. D. Lorenser, X. Yang, and D. D. Sampson, "Accurate modeling and design of graded-index fiber probes for optical coherence tomography using the beam propagation method," IEEE Photonics J. **5**(2), 3900015 (2013).
13. P. Tien, J. Gordon, and J. Whinnery, "Focusing of a light beam of gaussian field distribution in continuous and periodic lens-like media," Proc. IEEE **53**(2), 129–136 (1965).
14. S. G. Krivoshlykov and I. N. Sissakian, "Optical beam and pulse propagation in inhomogeneous media: Application to multimode parabolic-index waveguides," Opt. Quantum Electron. **12**(6), 463–475 (1980).
15. M. Newstein and B. Rudman, "Laguerre–Gaussian periodically focusing beams in a quadratic index medium," IEEE J. Quantum Electron. **23**(5), 481–482 (1987).
16. J. C. Gutiérrez-Vega and M. A. Bandres, "Ince–Gaussian beams in a quadratic-index medium," J. Opt. Soc. Am. A **22**(2), 306–309 (2005).
17. A. K. Ghatak and E. G. Sauter, "The harmonic oscillator problem and the parabolic index optical waveguide: I. Classical and ray optic analysis," Eur. J. Phys. **10**(2), 136–143 (1989).
18. E. G. Sauter and A. K. Ghatak, "The harmonic oscillator problem and the parabolic index optical waveguide: Ii. quantum mechanical and wave optical analyses," Eur. J. Phys. **10**(2), 144–150 (1989).
19. S. N. Khonina, A. S. Striletz, and A. A. Kovalev, et al. "Propagation of laser vortex beams in a parabolic optical fiber," in *Optical Technologies for Telecommunications 2009*, vol. 7523 (SPIE, 2009), p. 75230B.
20. O. A. Mossoulina, M. S. Kirilenko, and S. N. Khonina, "Simulation of vortex laser beams propagation in parabolic index media based on fractional Fourier transform," J. Phys.: Conf. Ser. **741**, 012142 (2016).
21. Y. Wu, J. Wu, and Z. Lin, "Propagation properties and radiation forces of the Hermite–Gaussian vortex beam in a medium with a parabolic refractive index," Appl. Opt. **59**(27), 8342–8348 (2020).
22. V. V. Kotlyar, A. A. Kovalev, and A. G. Nalimov, "Propagation of hypergeometric laser beams in a medium with a parabolic refractive index," J. Opt. **15**(12), 125706 (2013).
23. S. Cruz y Cruz and Z. Gress, "Group approach to the paraxial propagation of Hermite-Gaussian modes in a parabolic medium," Ann. Phys. **383**, 257–277 (2017).
24. L. Zhang, F. Deng, and Y. Peng, "Chirped Airy–Gaussian beam in a medium with a parabolic potential," Laser Phys. **27**(1), 015404 (2017).
25. F. Zang, Y. Ge, and Y. Wang, "Effect of initial chirp on the dynamics of the optical beam in a medium with parabolic potential," Appl. Phys. B **126**(10), 164 (2020).
26. K. Zhan, W. Zhang, R. Jiao, *et al.*, "Period-reversal accelerating self-imaging and multi-beams interference based on accelerating beams in parabolic optical potentials," Opt. Express **28**(14), 20007–20015 (2020).
27. J. Jia, H. Lin, and Y. Liao, "Pendulum-type light beams," Optica **10**(1), 90–96 (2023).
28. J. Jia, H. Lin, and S. Fu, "Shadows of structured beams in lenslike media," Opt. Express **31**(24), 40824–40835 (2023).
29. A. W. Snyder and J. D. Love, *Weak-guidance approximation* (Springer US, Boston, MA, 1983) 623–639
30. W. Chew, *Waves and Fields in Inhomogeneous Media, Electromagnetic waves* (IEEE Press, 1995).
31. M. P. Morales Rodríguez, O. S. Magaña-Loaiza, B. Perez-Garcia, *et al.*, "Coherent states of the Laguerre–Gauss modes," Opt. Lett. **49**(6), 1489–1492 (2024).
32. R. J. Glauber, "Coherent and incoherent states of the radiation field," Phys. Rev. **131**(6), 2766–2788 (1963).
33. E. C. G. Sudarshan, "Equivalence of semiclassical and quantum mechanical descriptions of statistical light beams," Phys. Rev. Lett. **10**(7), 277–279 (1963).

OPTICS CONTINUUM

34. A. Ruelas, J. A. Davis, and I. Moreno, "Accelerating beams with on-demand transverse shapes," Opt. Express **22**(3), 3490–3500 (2014).
35. R. Gilmore, "Geometry of symmetrized states," Ann. Phys. **74**(2), 391–463 (1972).
36. A. M. Perelomov, "Coherent states for arbitrary Lie group," Commun. Math. Phys. **26**(3), 222–236 (1972).
37. A. O. Barut and L. Girardello, "New "coherent" states associated with non-compact groups," Commun. Math. Phys. **21**(1), 41–55 (1971).
38. J. Joo, W. J. Munro, and T. P. Spiller, "Quantum metrology with entangled coherent states," Phys. Rev. Lett. **107**(8), 083601 (2011).
39. B. J. Lawrie, P. D. Lett, A. M. Marino, *et al.*, "Quantum sensing with squeezed light," ACS Photonics **6**(6), 1307–1318 (2019).
40. C. Cohen-Tannoudji, B. Diu, and F. Laloë, *Quantum mechanics*; 1st ed. (Wiley, New York, NY, 1977).
41. F. E. Onah, E. García Herrera, J. A. Ruelas-Galván, *et al.*, "Quadratic time-dependent quantum harmonic oscillator," Sci. Rep. **13**(1), 8312 (2023).
42. S. Van Enk and G. Nienhuis, "Eigenfunction description of laser beams and orbital angular momentum of light," Opt. Commun. **94**(1-3), 147–158 (1992).
43. C. C. Gerry, "Correlated two-mode *SU*(1, 1) coherent states: nonclassical properties," J. Opt. Soc. Am. B **8**(3), 685–690 (1991).
44. C. Brif, A. Vourdas, and A. Mann, "Analytic representations based on SU(1,1) coherent states and their applications," J. Phys. A: Math. Gen. **29**(18), 5873–5885 (1996).
45. M. Novaes, "Some basics of su(1,1)," Rev. Bras. Ensino Fis. **26**(4), 351–357 (2004).
46. B. L. Schumaker and C. M. Caves, "New formalism for two-photon quantum optics. II. Mathematical foundation and compact notation," Phys. Rev. A **31**(5), 3093–3111 (1985).